ELSEVIER

Tectonophysics 299 (1998) 213–227

TECTONOPHYSICS

Polyphased block tectonics along the North Anatolian Fault in the Tosya basin area (Turkey)

Damien Dhont [a,*], Jean Chorowicz [a], Tekin Yürür [b], Onur Köse [b]

[a] *Département de Géotectonique, ESA–CNRS 7072, case 129, Université Paris 6, 4 place Jussieu, 75252 Paris, cedex 05, France*
[b] *Department of Geology, Hacettepe University, Beytepe, Ankara, Turkey*

Received 2 October 1997; accepted 21 April 1998

Abstract

The Tosya basin is located in the bending segment of the North Anatolian Fault (NAF) in Turkey. We have obtained original observations on the neotectonics from SAR ERS images, Digital Elevation Model (DEM) and field structural analysis. Regional Neogene deformation is characterised by the occurrence of several basins that are superimposed in time and space. They result from differently oriented movements since 12 Ma, including southwestward motion along a fault subparallel to the NAF. We propose a model of polyphased tectonics related to the displacement of several individualised blocks. In the first stage (Tortonian), the North Tosya block has moved toward the N250º azimuth, parallel to the dextral N70º-striking segment of the NAF. As a consequence, a triple-junction-related compatibility basin was opened at the intersection with a N60º to N30º-striking fault. This pattern is similar to the Karliova corner where the NAF and the East Anatolian Fault meet. In the second stage (Early Pliocene–Middle Pleistocene), a segment of the former N70º-NAF was abandoned and the NAF propagated eastward to form a N90º-striking segment (N90º-NAF), cutting the former Tosya block and basin into two parts. The North Tosya block has moved again and this new geometry has permitted a South Tosya block to move parallel to the NAF but with a higher rate which has induced compression in the Tosya basin. In the third stage (Holocene), the South Tosya block moved toward N240º, obliquely to any of the NAF segments. This has resulted in the formation of two Holocene pull-apart type basins along the previous N60º to N30º-striking fault while extensional faults were formed in the South Tosya block. Estimated dextral displacement along the NAF is 5.9 to 8.5 km at this stage. This model of blocks moving in different directions, including Holocene local movements toward N240º, means that the NAF can be considered not to be a simple transform fault. Our model implies that the N90º-NAF was non-existent before the Early Pliocene.

Keywords: North Anatolian Fault; neotectonics; block tectonics; strain; fault propagation; pull-apart

1. Introduction

The North Anatolian Fault (NAF) is the 1500-km-long boundary between Anatolia and Eurasia (Fig. 1). The NAF was initiated during the Neogene in the context of continental collision between Arabia and Eurasia. Anatolia (the Anatolian plate) is extruded westward between the NAF and the sinistral East Anatolian Fault (EAF) since the Serravalian–Tortonian at c. 12–13 Ma (McKenzie, 1972; Sengör et al., 1985; Dewey et al., 1986). Barka (1992) has summarised published works on both age and amount of total motion of the NAF. The estimate of movement initiation

* Corresponding author. Tel.: +33 144 275089; Fax: +33 144 275085; E-mail: damien@igs.jussieu.fr

0040-1951/98/$ – see front matter
PII: S0040-1951(98)00206-6

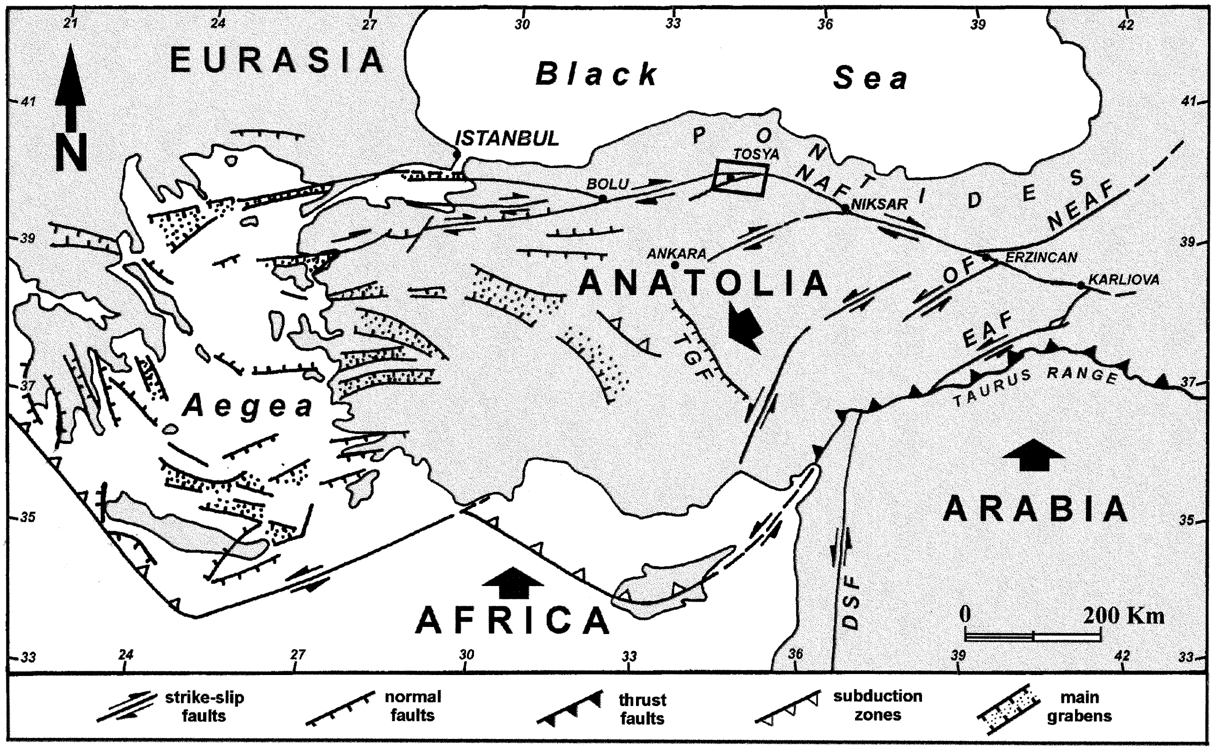

Fig. 1. Geodynamic context of Turkey (modified from Sengör, 1979; Hancock and Barka, 1981; Dewey et al., 1986; Chorowicz et al., 1994, 1995). Darkened frame along the North Anatolian Fault is the studied area. Large black arrows represent relative plate motions within the Eurasian reference. *DSF* = Dead Sea Fault; *NAF* = North Anatolian Fault; *EAF* = East Anatolian Fault; *NEAF* = North East Anatolian Fault; *OF* = Ovacik Fault; *TGF* = Tuz Gölü fault.

ranges from Late Miocene to Early Pliocene, and that of finite displacement from 25 ± 5 km to 350 to 400 km. Barka (1992) has concluded that motion initiation along the NAF has started in the Early Pliocene at c. 5 Ma and that there is a decrease in total displacement along its trace from 40 ± 5 km near Erzincan in the east to 25 ± 5 km near Bolu in the west.

Extension induced by the Aegean back-arc basin affects the Anatolian plate as far in the east as the Tuz Gölu fault region (Sengör et al., 1985; Dhont et al., 1998). The NAF is considered a curved (concave to the south) intracontinental transform fault which permits counterclockwise rotation of the Anatolian plate relative to the Eurasian plate (Le Pichon et al., 1995; Oral et al., 1995; Reilinger et al., 1997). This model implies that movement in the northern part of the Anatolian block is parallel to the NAF.

To test this model, we have examined its compatibility with local tectonic features within the region where the strike of the NAF progressively turns from N70° in the west to N90° in its central part. We have focused our work on the Tosya area (Fig. 1). Polyphased tectonics has been described along this fault segment (Hancock and Barka, 1981; Barka and Hancock, 1984; Barka, 1985; Över et al., 1993; Andrieux et al., 1995; Bellier et al., 1997) and we want to show that local scale blocks have moved in different directions during several neotectonic events.

Fault mapping can be carried out using new data such as images of a Digital Elevation Model (DEM) at pixel size 200 m, completed by images of the Synthetic Aperture Radar (SAR) of the European Remote Sensing (ERS) satellite at pixel size 12.5 m. Both DEM and SAR ERS images express landforms and have synoptic views permitting detailed mapping of the neotectonic features over large surfaces, giving the geometry of the regional deformation (Chorowicz et al., 1994, 1995). As a complement, field structural analysis provides information on the mechanisms of the deformation.

We first describe the regional structural framework of the area. Afterward, we present the data and the methodology. Mapping of the neotectonic features is exposed in Section 4, before discussion and proposition of a new geodynamic interpretation. We finally estimate finite displacement values along the NAF over the past 12 Ma.

2. Regional structural framework

The studied area comprises the Tosya and Kargi basins. They are filled by sediments of the Pontus unit, ranging in this region from Tortonian (12 Ma) to middle Pleistocene. Ages are based on Barka and Hancock's analysis (1984) of faunal/floral assemblages, correlated to the lithostratigraphic scale of Irrlitz (1971, 1972). The Pontus unit is formed of two rock units separated by an unconformity of Messinian age (Fig. 2) which angle decreases with distance from the NAF. The lower Pontus unit, attributed to the Tortonian (Irrlitz, 1972; Barka and Hancock, 1984) or to the Pliocene (Över, 1996; Bellier et al., 1997), is mainly made of lacustrine deposits. In the Kargi basin it consists of marls, lacustrine limestone and calcareous matrix conglomerate. In the Tosya basin, it consists of basal conglomerate, lacustrine limestone, sand, marls and silty clay. The upper Pontus unit, mainly made of fluvial deposits, begins in the Pliocene and ends in the middle Pleistocene. The fluvial deposits are silt and conglomerate in the Kargi basin, and coarse conglomerate or ochrous silty clay in the Tosya basin. Along the northern border of the Tosya basin, the bottom of the upper Pontus unit is conglomeratic, attesting that an active palaeorelief has provided the clastic elements during fault motion.

The Pontus unit unconformably lies upon basement rocks consisting of metamorphic schist, Neotethyan ophiolites and related melange. In the Tosya basin, volcanogenic sediments of the Devrez Cay Formation, dating Early to Middle Miocene (Barka and Hancock, 1984), are located between the Pontus layers and the basement rocks.

Different successions of stress patterns have been described for the Neogene–Quaternary time within the arc of the NAF (Hancock and Barka, 1980, 1981; Barka and Hancock, 1984; Över et al., 1993; Andrieux et al., 1995; Bellier et al., 1997) but no mechanism of basin opening has to-day been proposed.

3. Images and methodology

3.1. Images

The Digital Elevation Model (DEM) was generated from digitisation of contour lines of two topographic maps at a scale of 1 : 250,000. It covers 100×40 km^2 at 200 m horizontal ground resolution. The DEM was processed in order to produce shadowed images illustrating the major geomorphic features of the studied area (Fig. 3a, b).

The SAR ERS-1 images (Figs. 4 and 7) were generated from original tapes by standard processing including linear stretching. The scenes cover 100×100 km^2, at 12.5 m ground resolution. ERS is a polar satellite which can operate both in descending (from north to south, looking west) or ascending (from south to north, looking east) orbits. We have produced positive or negative prints. In negative prints, slopes facing the radar are expressed in black whereas detailed information is well exposed by various grey tones in the slopes backing illumination.

3.2. Methodology

Analysis of DEM and SAR images is based on the observation of landforms resulting from the neotectonics, principally fault scarps, subsiding low plains and high relief. These images, artificially or originally obliquely illuminated, express variations in topographic slopes. Distinction between active and non-active fault scarps is more efficient in stereoscopic views. Except its central part, the image of Fig. 4 overlaps scenes of adjacent orbits. We have analysed these stereopairs in order to observe the geometry of basins along the NAF. We first analysed the DEM images (Fig. 3c), then the radar images (Fig. 4) which we have systematically compared with the DEM. We mapped only the active faults, determined as such because they cut the Late Miocene to Quaternary sediments or are poorly eroded. All the tectonic features have been collected to form a complete map (Fig. 5).

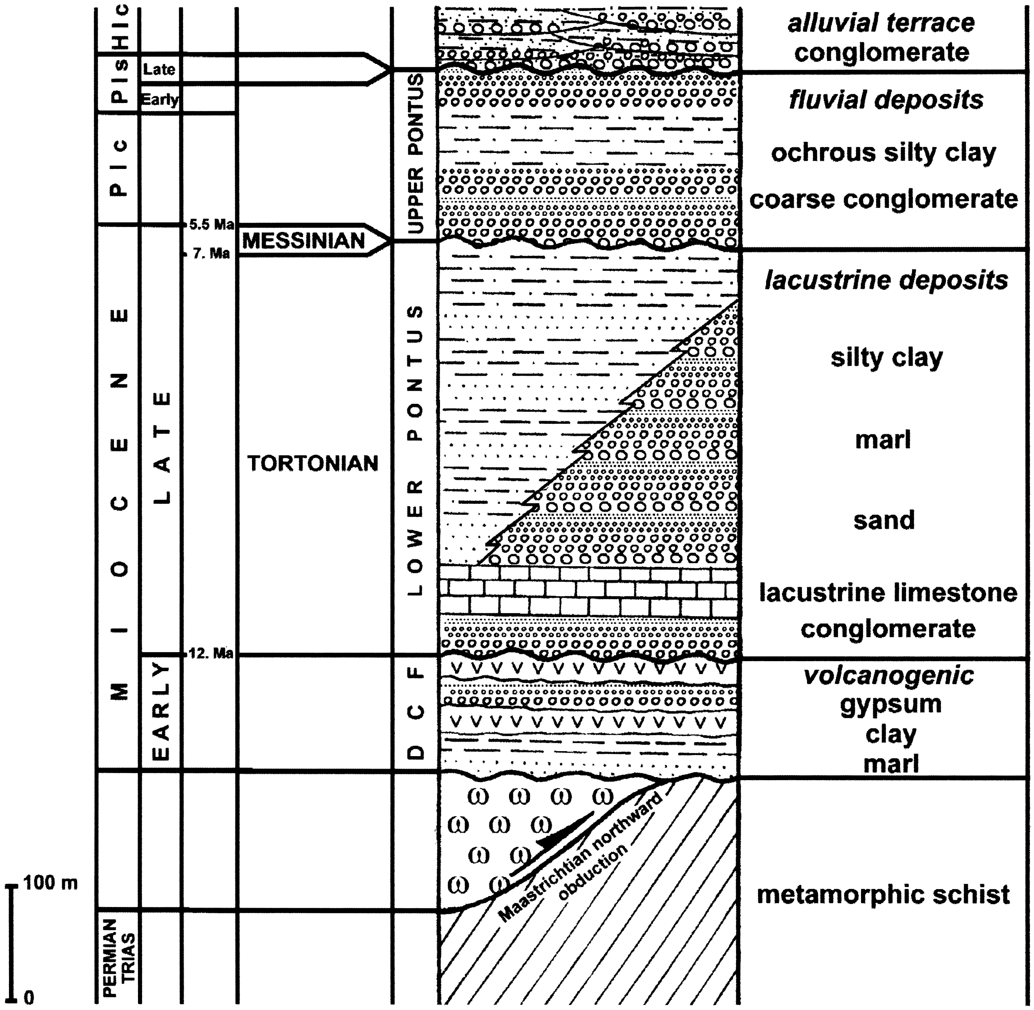

Fig. 2. Lithostratigraphic columnar section of the Quaternary, Neogene and pre-Neogene formations of the Tosya area (from Barka, 1992; Över et al., 1992; Andrieux et al., 1995). *DCF* = Devrez Cay Formation; *Hlc* = Holocene; *Plc* = Pliocene; *Pls* = Pleistocene; ω = ophiolites and mélange.

Field structural analysis consists of measurements of orientation and sense-of-motion of striated fault planes, and attitude of tension fractures, distributed in seventeen sites (Figs. 5 and 6). In order to favour the indications of movement, special emphasis has been put on striations directly observed on major (mapped) fault planes along which the main parts of the regional displacements have occurred. For this reason, we plotted in Fig. 5 the plunge of striations measured directly on the main plane of mapped faults or on nearby smaller faults parallel to the major one. Along normal faults the azimuth

Fig. 3. Interpretation of the Digital Elevation Model (DEM) of the studied area. (a, b) DEM images generated by linear interpolation from digitisation of elevation contour lines of two maps at 1 : 250,000 scale. Ground resolution is 200 m. Illumination is (a) from north and (b) from west. (c) Structural interpretation of the DEM images; *l* = landslides. (See legend of Fig. 5 for meaning of letters.)

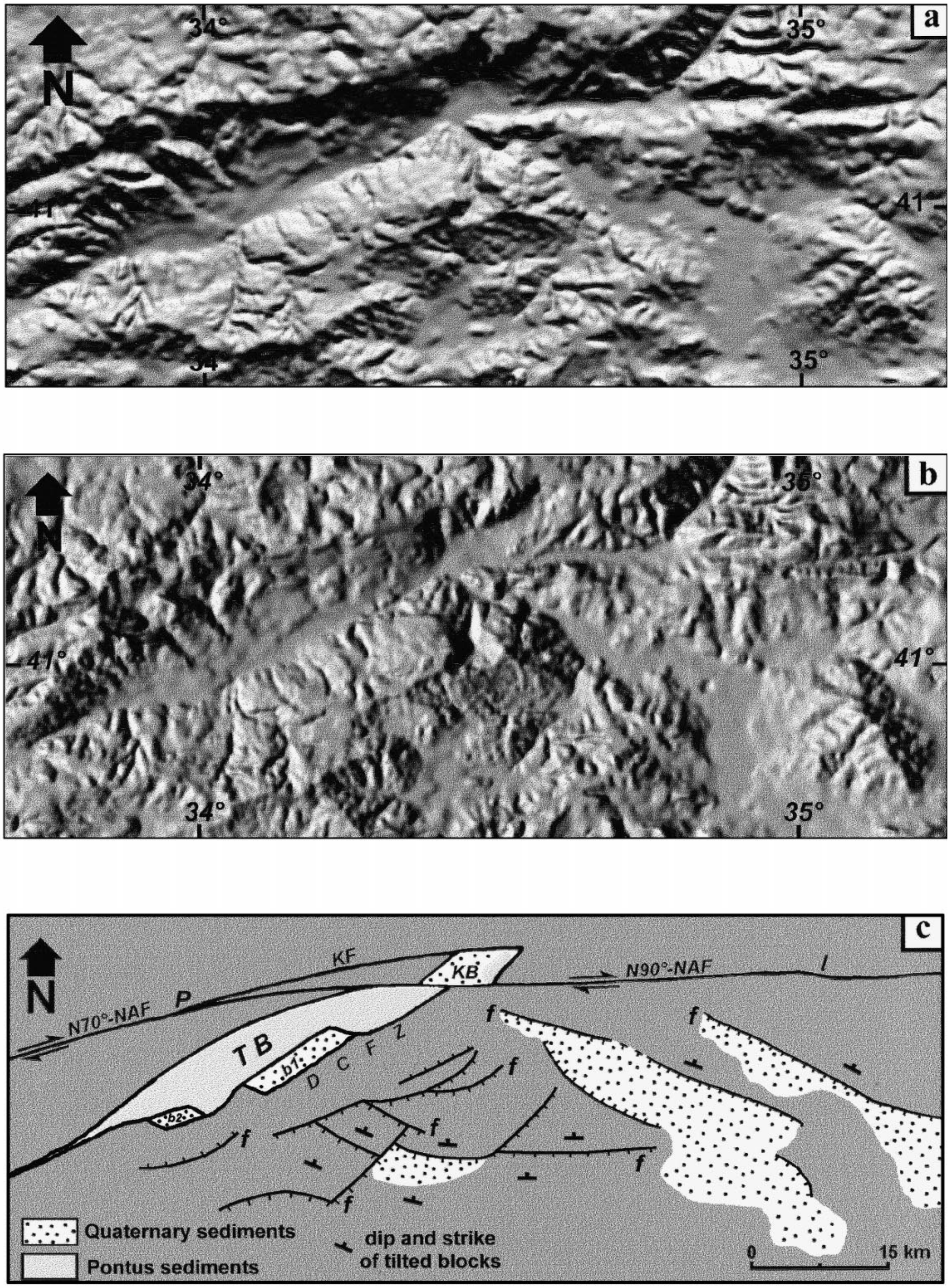
a
34°
35°
N
41°
b
34°
35°
N
41°
c
N
KF
KB
N90°-NAF
P
N70°-NAF
TB
b1
D C F Z
b2
f
Quaternary sediments
Pontus sediments
dip and strike
of tilted blocks
0
15 km

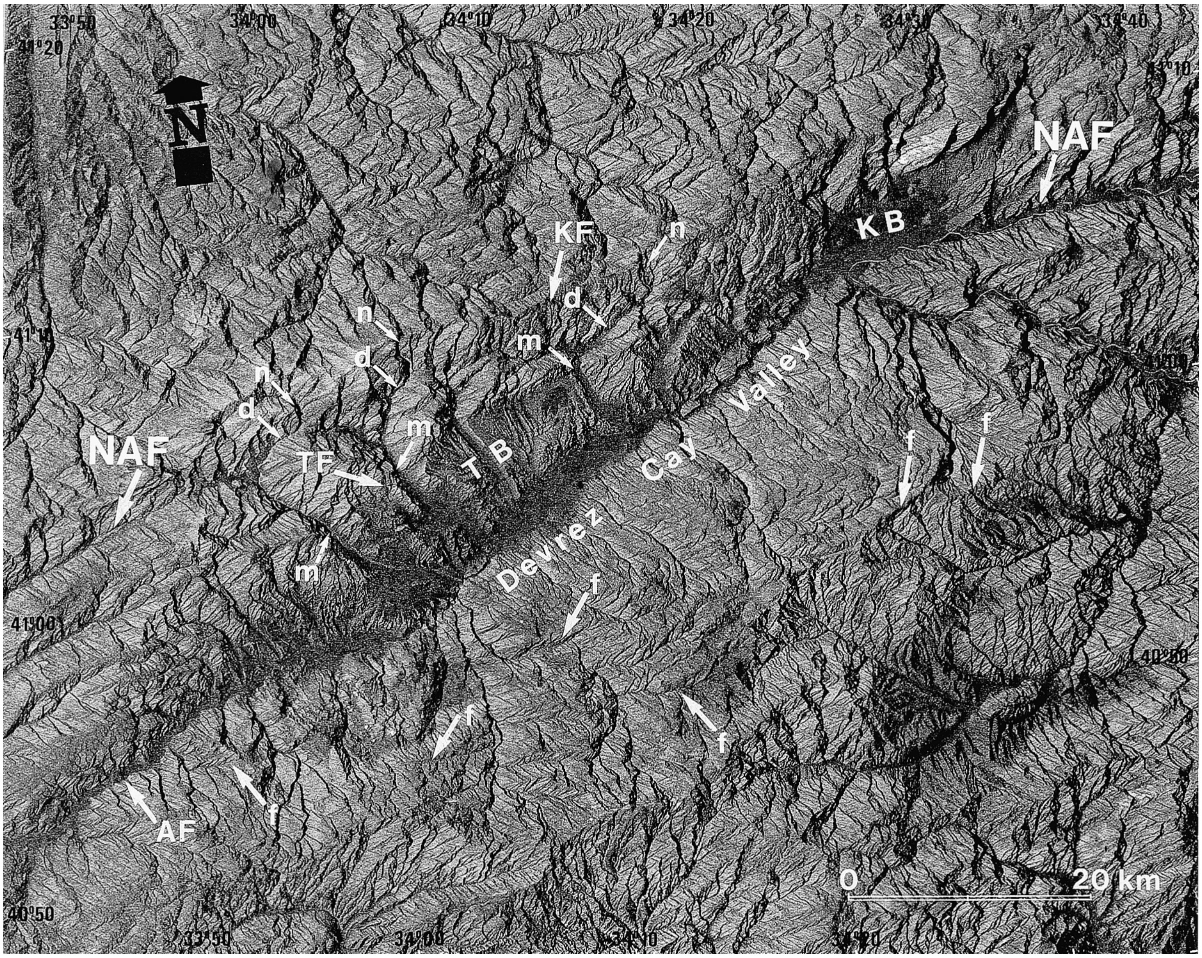

Fig. 4. SAR ERS-1 image of the Tosya area (negative print, descending orbit, radar illumination from the east). (See legend of Fig. 5 for meaning of letters.)

of the plunge indicates the horizontal component of local displacement.

Striations are dated as Recent when they affect Recent (Late Miocene to Quaternary) rocks. By places, we also took into consideration striations affecting basement rocks, but only along the major Recent faults characterised by distinct geomorphic expression. There we generally found only one set of striations, which we have supposed to be related to the latest displacement.

When measurements were taken in sites that are not located along major mapped faults, we took into account only the striations affecting late Neogene rocks, including sediments filling open faults in sites 1, 2, 7, 10 and 11. We have used the striations on the various fault planes to compute the orientation of the regional palaeostress pattern (Angelier, 1990). We suppose that local strain due to minor faults is related to a single regional palaeostress pattern. When several deformation events where assumed, we employed the 4-D method of Angelier (1984) to classify superimposed deformations. This method uses an estimate of the discrepancy between each striation measurement and the computed theoretical slip vector, permitting to appreciate their compatibility either with one or several phases of deformation. The value of parameter PHI $\left[(\sigma_2 - \sigma_3)/(\sigma_1 - \sigma_3)\right]$ gives the stress ellipsoid shape which has three well distinct axes when PHI-values are close to 0.5. A PHI-value approaching 0 indicates that norm value

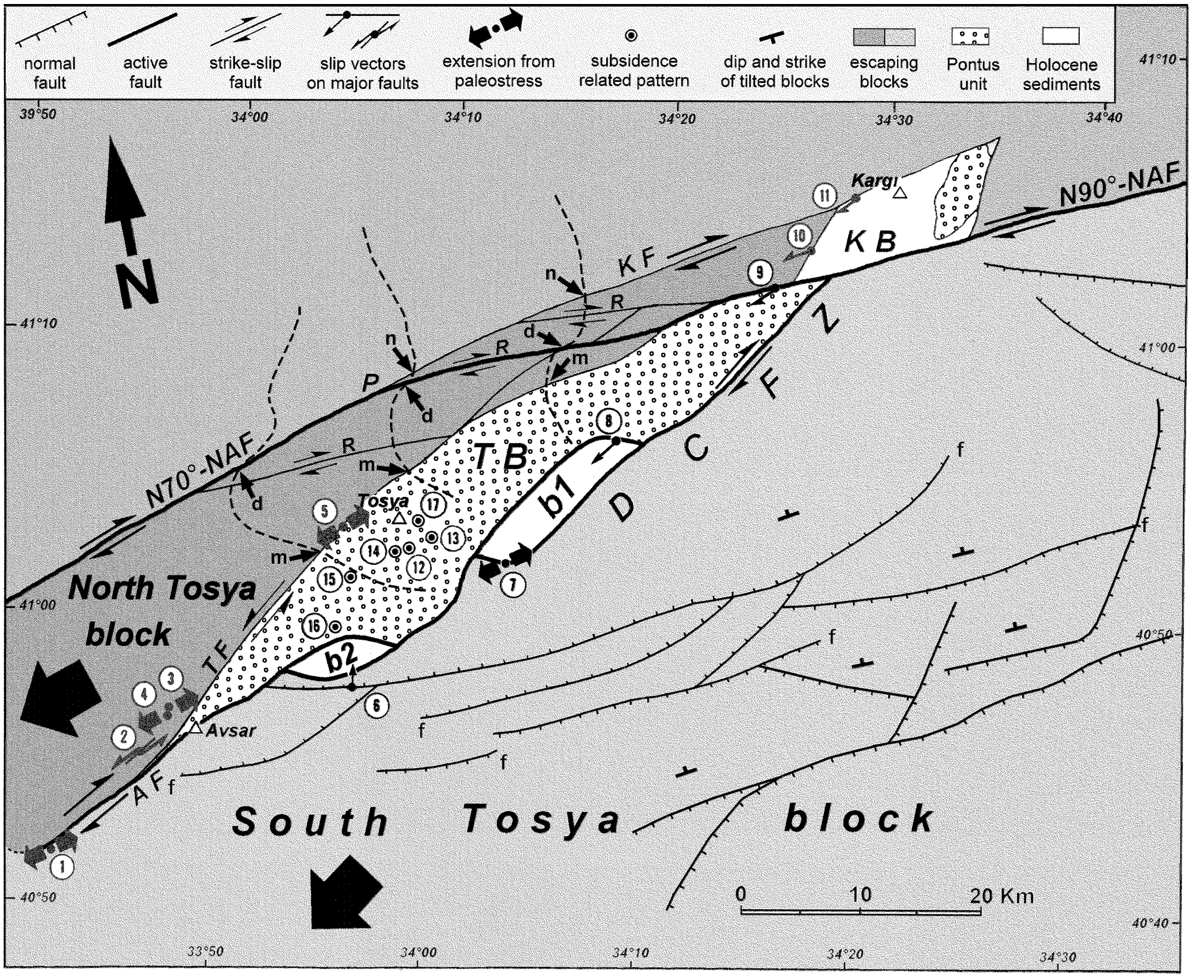

Fig. 5. Structural interpretation of the SAR ERS-1 image of Fig. 4: *b1* and *b2* = Holocene pull-apart type basins; *AF* = Avsar fault; *DCFZ* = Devrez Cay fault zone; *f* = extensional faults bounding tilted blocks; *KB* = Kargi basin; *KF* = Kargi fault; *NAF* = North Anatolian fault; *P* = meeting point of the N70°-NAF and the N90°-NAF; *R* = Riedel faults associated to the dextral strike-slip component of the NAF; *TB* = Tosya basin; *TF* = Tosya fault. Encircled numbers are sites of structural analysis (see Fig. 6). Dashed lines are main valleys dextrally displaced by the NAF (*d*) while they are not offset by the Kargi fault (*n*) and the Tosya fault (*m*). Grey and black arrows are slip vectors and extension patterns related to motions respectively during Pontus and Holocene times.

of σ_3 is close to σ_2, and can be interpreted as a tectonic subsidence pattern.

4. Mapping of neotectonic features

4.1. North Anatolian Fault

The synoptic views of the DEM images have permitted to follow the main trace of the NAF, which is defined by its continuity (Fig. 3a, b). The trace is well expressed in the east as a straight structural valley. Seismic activity is characterised by the 1943 earthquake (Barka, 1996; Stein et al., 1997). Figs. 3 and 7 show that the NAF consists of two differently oriented strands meeting at point P. West of P, the NAF is clearly identified by a sharp scarp trending N70°. East of P, the NAF divides into two branches. The northern one (KF, the Kargi fault) has a discrete N80°-trending trace and ends eastward along

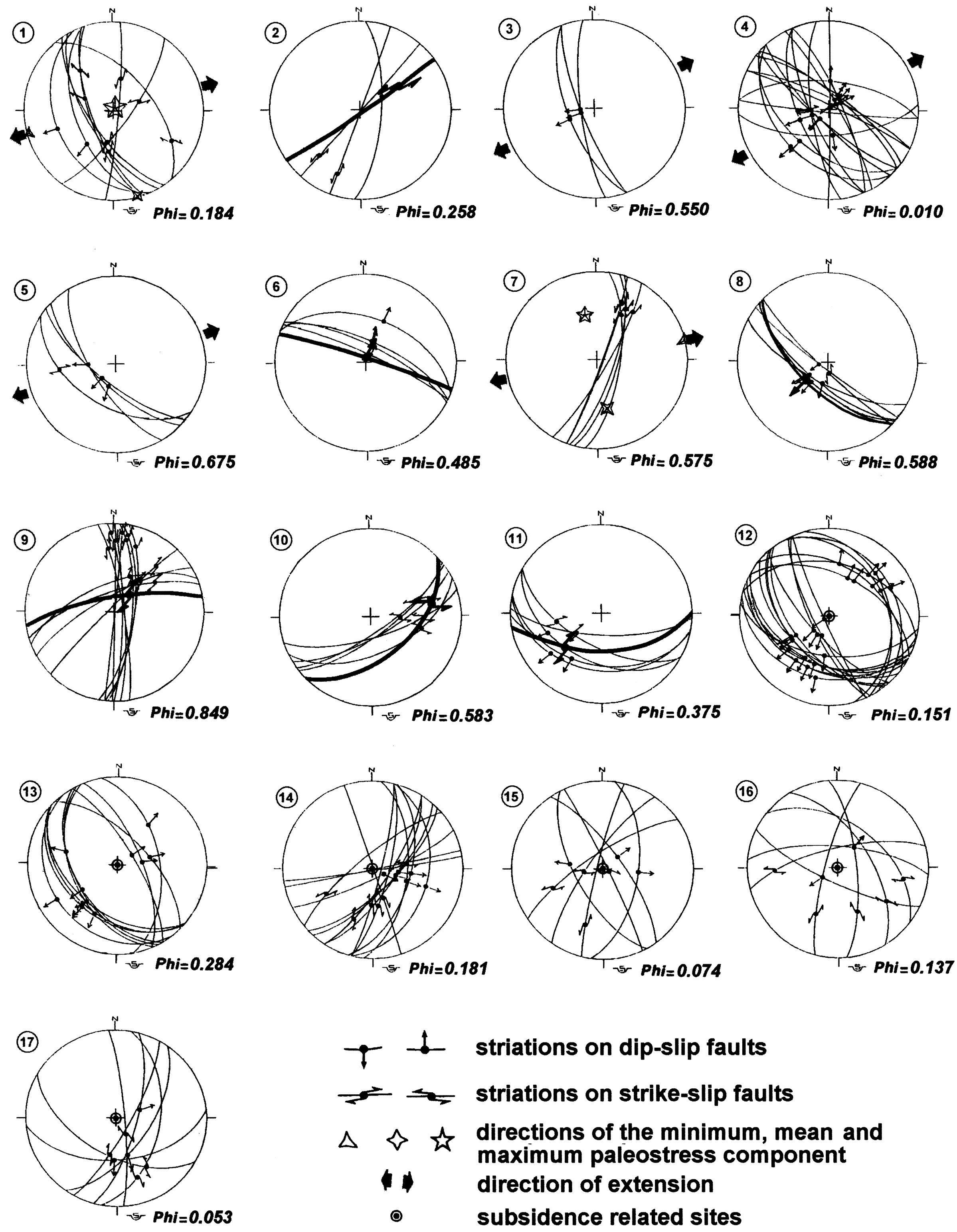
1
Phi= 0.184
2
Phi= 0.258
3
Phi= 0.550
4
Phi= 0.010
5
Phi= 0.675
6
Phi= 0.485
7
Phi= 0.575
8
Phi= 0.588
9
Phi= 0.849
10
Phi= 0.583
11
Phi= 0.375
12
Phi= 0.151
13
Phi= 0.284
14
Phi= 0.181
15
Phi= 0.074
16
Phi= 0.137
17
Phi= 0.053
striations on dip-slip faults
striations on strike-slip faults
directions of the minimum, mean and maximum paleostress component
direction of extension
subsidence related sites

the northern border of the Kargi basin. The southern one (N90º-NAF) continues in the N90º direction as a straight line, sometimes covered by landslides (l in Fig. 3c). To support our analysis we present a stereopair of radar images (Fig. 7) picturing the Kargi fault and its intersection with the NAF at point P. The evidence is that the Kargi fault has an eroded scarp (many gullies, low and smoothed scarp), whereas the NAF has a locally steeper scarp, a distinct trace and the gully system is less developed. Main valleys crossed by the fault zone are dextrally displaced by the NAF (d in Figs. 4, 5 and 7) whereas they are not offset by the Kargi fault (n in Figs. 4, 5 and 7). Compared to the N70º-NAF, its alongstrike prolongation (the Kargi fault) is morphologically less distinct and consequently an old, inactive branch of the NAF. The high ground resolution radar images have permitted more detailed mapping and show in the North Tosya block a series of E-striking en-echelon faults branching on the N70º-NAF. Barka and Hancock (1984) have interpreted these faults as Riedel faults (R in Figs. 5 and 7) associated to dextral strike-slip movement of the NAF. Measurements in site 9 taken on faults affecting lower Pontus lacustrine limestone show that the horizontal slip along the NAF is not pure dextral strike-slip but rather transtensive, at least during the Neogene.

4.2. Tosya basin

The Tosya basin is separated in the north from the Kargi basin by the N90º-NAF (Figs. 3–5). Recent sediments form flat surfaces on the basin floor surrounding hilly low relief which corresponds to the Pontus unit.

The basin comprises two small rhomb-shaped, flat-bottomed Holocene basins (b1, b2, Fig. 3c and Fig. 5). The main Tosya basin is hilly and infilled by Pontus rocks. It is bounded in the north by the N90º-NAF, in the south by the Avsar fault (AF in Fig. 5) paralleling the N70º-NAF, in the northwest by the Tosya fault (TF) forming a large curved scarp, and in the southeast by the Devrez Cay fault zone (DCFZ) striking N60º to N30º. The DCFZ and Avsar fault can be considered as active because they form the most evidenced scarps of the region (Fig. 4), whereas the Tosya fault is inactive because main valleys cutting across are not offset (m in Figs. 4, 5 and 7). Striation along or close to the Tosya fault in sites 2, 3* and 4* in volcanic series of the Devrez Cay Formation (Early Miocene), and in site 5* in conglomerate of upper Pontus age, show WSW–ENE extension occurring during and/or after late Pontus time. This direction of extension is compatible with sinistral strike-slip motion along the Tosya fault. Site 1 is located in the Devrez Cay Formation along the Avsar fault, which can be considered as a reactivated segment of the Tosya fault. Striated normal faults, infilled by late Pontus silty clays, give a WSW-trending σ_3, consistent with the previous left-lateral movement along the Tosya fault in the late Pontus. In site 7, late Pontus clays wedged into Neotethyan ophiolitic mélange are affected by N10º–N20º sinistral strike-slip faults indicating WSW–ENE extension along the DCFZ, at least during the late Pontus. Moreover, as clearly expressed on the DEM images (Fig. 3) and on the radar stereopair (Fig. 7), the steep Devrez Cay valley slopes are distinct scarps which indicate recent tectonic activity.

More to the south, basement and volcanic rocks of the Devrez Cay Formation are cut by faults striking NE–SW to E–W (f in Figs. 3–5) having a curved shape compatible with normal listric-faulting geometry. In site 6* (Figs. 5 and 6), striation measurements taken along one of these faults in the volcanic sediments of the Early Miocene Devrez Cay Formation indicate dip-slip movement that confirms the N–S extension mechanism. More to the east, the DEM clearly expresses Quaternary depressions. They are best observed on the DEM of Fig. 3a where the fault-bounding tilted blocks are revealed by shadow (see dip and strike symbols on the figure). The b2 depression has a clear rhomb-shaped geometry and is located at a right stepping bend of the DCFZ. The b1 basin is well expressed in Fig. 4 and also

Fig. 6. Data from field structural analysis. Schmidt nets, lower hemisphere. For site locations (number in circle) see Fig. 5. Thick lines are plots of major (mapped) faults and related striations. Sites 3, 4, 5 and 6 are taken from Över et al. (1992) and marked by * in the main text.

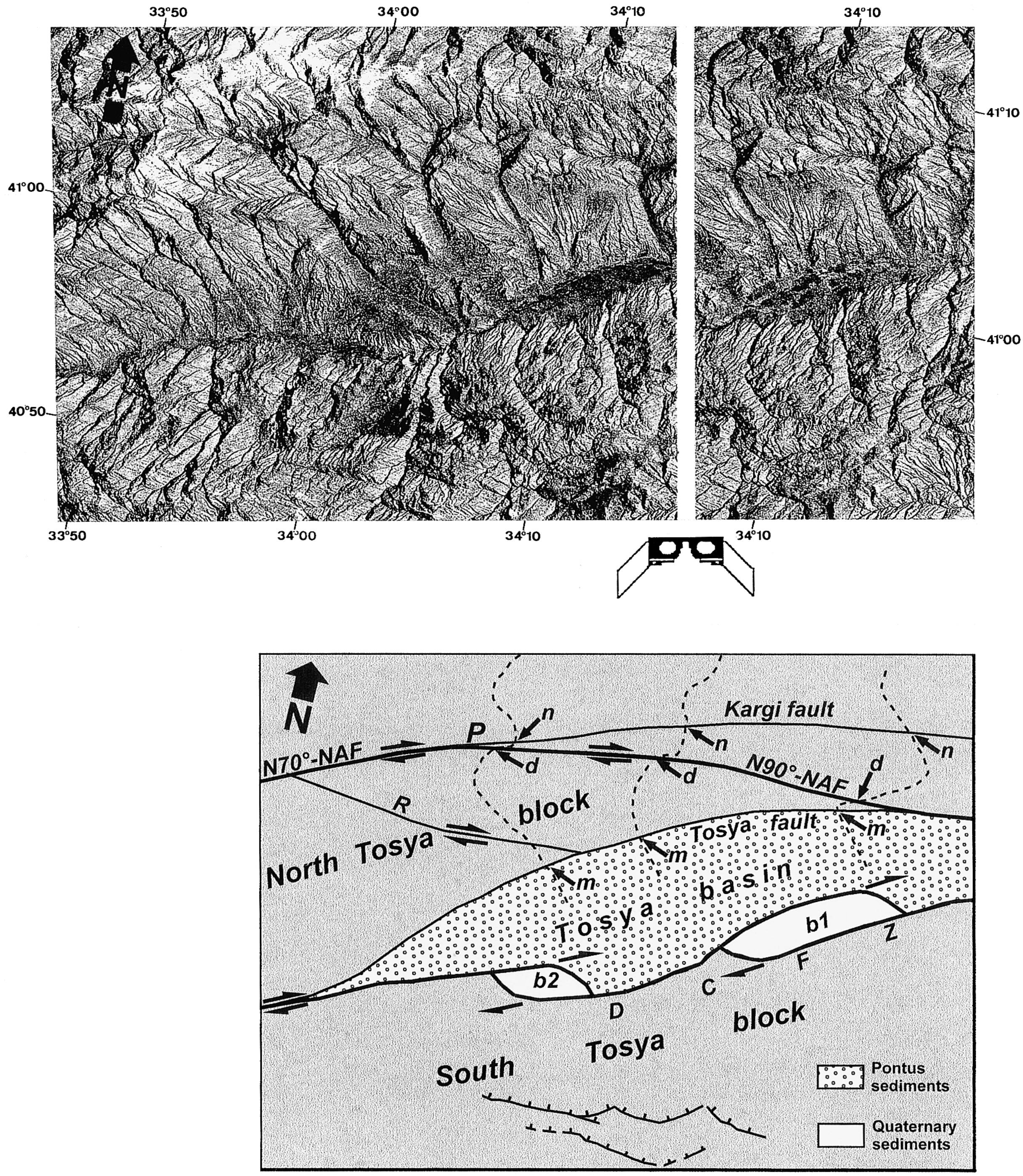

Fig. 7. Sample of stereopair of radar images (ascending orbits, radar illumination from the west) showing the P intersection of the NAF and the Kargi fault. Same legend as Fig. 5.

exhibits a rhomb-shaped geometry located at a releasing bend of the DCFZ. We interpret b1 and b2 as pull-apart type basins, as suggested by Suzanne et al. (1990). Whatever the erosion processes can be, obvious along the Devrez Cay river, it is necessary to call for local subsidence in order to explain the b1 and b2 alluvial plains.

4.3. Kargi basin

The Kargi basin is bounded to the north by the Kargi fault (KF in Fig. 3c and Fig. 5), which is presently inactive as evidenced by its eroded scarp, and to the south by the N90º-NAF. The eastern and western borders are fault scarps striking N50º. Striations in sites 10 and 11 (Figs. 5 and 6), located respectively along the western and northern borders, were taken along faults infilled by ochrous clays belonging to the lower Pontus series and affecting schist rocks of the basement. They indicate E–W and ENE–WSW displacements compatible with respectively normal and dextral movements along the western and northern border faults. Holocene deposits infill most of the area but hilly Pontus series outcrop along the eastern side.

5. Discussion

The Holocene b1 and b2 pull-apart type basins have been formed by dextral strike-slip movements along the N60º-to-N30º-striking DCFZ. In site 8 (Figs. 5 and 6), striation measurements taken on fault planes affecting Holocene reddish clays indicate SW-directed motion along the northern border of the b1 basin. Data in sites 1 and 7 confirm that horizontal SW-directed finite displacement along the DCFZ is of regional scale. The DCFZ is the northwestern border of the South Tosya block which was consequently moving toward the N240º azimuth during the Holocene. Such block displacement would normally open along the N90º-NAF a transtensive zone which does not exist. We consequently interpret that the Holocene basins and the E-to-NE-striking extensional faults lying south of the N90º-NAF (Figs. 3 and 4) absorb the extension within the South Tosya block. Thus, extension related to motion of the South Tosya block is expressed by deformation inside the block and not by transtensional opening along the N90º-NAF.

In this interpretation, we have considered that the Kargi basin has not suffered extension during the Holocene. However, occurrence of lower Pontus sediments outcropping in the eastern part of the basin suggests an earlier opening. The Tosya basin, being infilled with the same lower Pontus layers, is coeval. By counterbalancing 12 km dextral offset along the N90º-NAF, the two basins perfectly fit. Hence, we interpret that the Tosya and Kargi basins were formed as a single basin during early Pontus time (Fig. 8a). They are now cut and displaced by the NAF. Surrender of the Kargi fault and transmission of the dextral strike-slip movement from the N70º-NAF to the N90º-NAF during late Pontus time are more realistic if the N90º-NAF is inherited from a previous R fault in the North Tosya block.

Opening of a single lower Pontus basin is made possible by N250º-directed motion of the North Tosya block along the dextral strike-slip N70º-NAF/Kargi fault system. This implies that the N240º-striking DCFZ might be left-lateral during early Pontus time. This assumption is consistent with the fact that the Late Miocene extension in the North Tosya block trends N250º (Fig. 5). The northeastern prolongation of the DCFZ was the eastern border of the Kargi basin (Fig. 8a). This system is similar to that of Karliova at the eastern end of the NAF were the EAF and the NAF meet to form a triple-junction geometry within which escape of the Anatolian block results in the formation of the Plio–Quaternary Karliova intermontane sedimentary basin (Dewey et al., 1986). During this stage, the NAF can be assimilated to a proto-NAF corresponding to the N70º-NAF and the Kargi fault segment. Motion of the North Tosya block has initiated dextral strike-slip Riedel faults, as clearly expressed on the radar images (R in Figs. 5 and 7). One of the Riedel faults has been reactivated during the late Pontus to form the active N90º-NAF which has cut the former lower Pontus basin into two parts and separated the Tosya and Kargi basins (Fig. 8b).

Compressional structures such as folds and thrusts involving upper Pontus rocks have been described and mapped in the Tosya basin (Andrieux et al., 1995). In our model, this tectonic setting can be explained by globally westward faster movement of

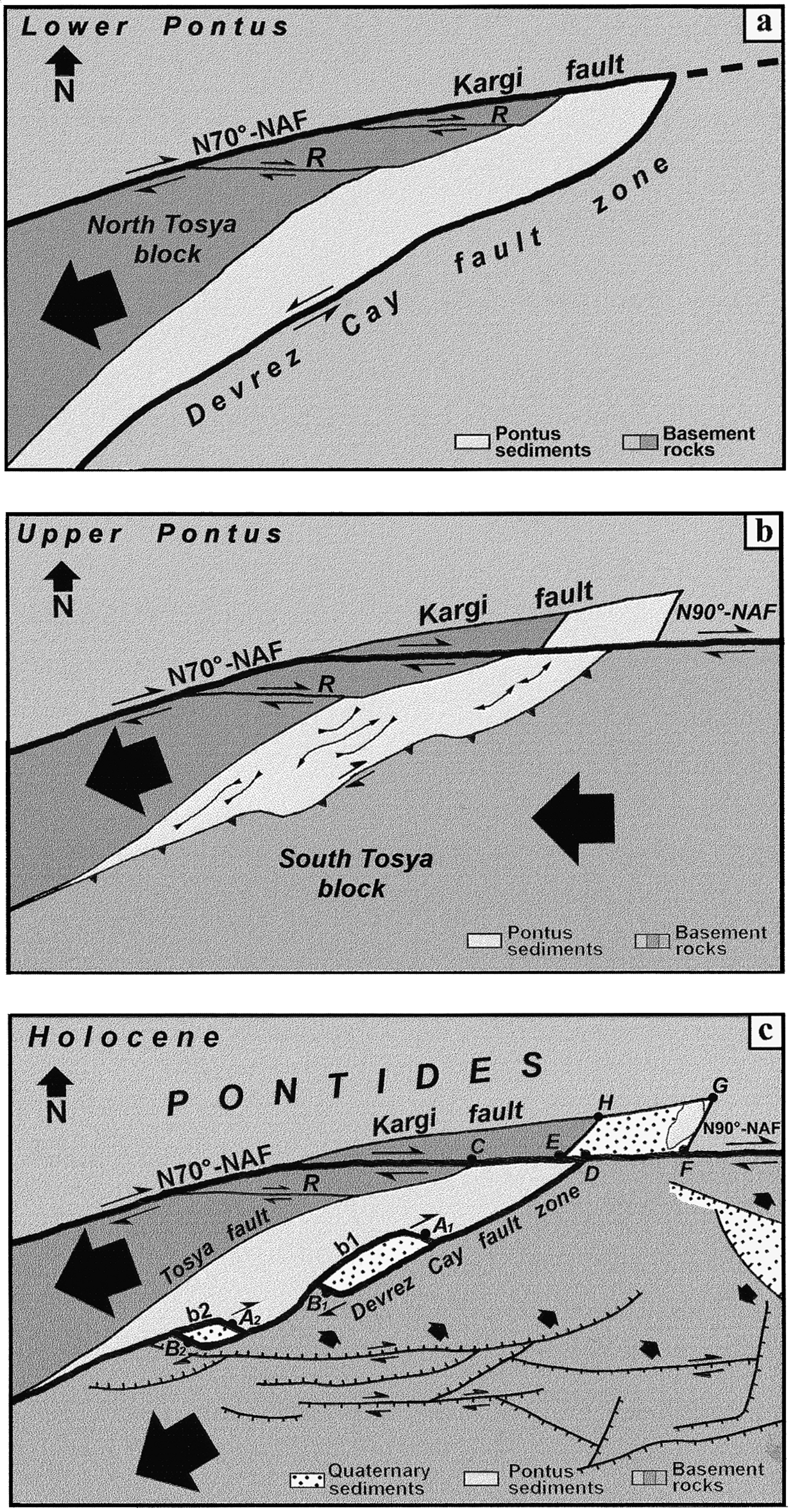
a
Lower Pontus
N
Kargi fault
N70°-NAF
R
R
North Tosya block
Devrez Cay fault zone
Pontus sediments
Basement rocks
b
Upper Pontus
N
Kargi fault
N90°-NAF
N70°-NAF
R
South Tosya block
Pontus sediments
Basement rocks
c
Holocene
N
PONTIDES
Kargi fault
H
G
N90°-NAF
C
E
D
F
N70°-NAF
R
Tosya fault
Devrez Cay fault zone
b1
A1
B1
b2
A2
B2
Quaternary sediments
Pontus sediments
Basement rocks

the South Tosya block relative to the North Tosya one, rather inducing transpression within the Tosya basin.

6. New geodynamic interpretation

One of the most important facts described above is the occurrence of two Holocene pull-apart type basins impinged onto the older Tosya basin, implicating a complex evolution of the area. We present below a three-stage model. The first stage, dated as early Pontus, was the formation of a basin in between the NAF/Kargi fault system and the DCFZ (Fig. 8a). This was made possible by the N250º-directed relative displacement of the North Tosya block in between these two faults. WSW-ward motion of the North Tosya block induced formation of dextral en-echelon faults. Geometry of a block moving in between to conjugate strike-slip faults generates a triple-junction compatibility basin similar to that of the eastern end of the NAF at Karliova, where the Anatolian block escapes between the NAF and the EAF. Motion of the North Tosya block is related to the extension in the Aegean Sea which concerns large areas in Anatolia up to Tosya (Bellier et al., 1997) and possibly beyond to the east (Sengör et al., 1985). At that time, the angle between the NAF and the DCFZ was larger than now (Fig. 8a) but was significantly reduced during the compressional second stage. This second stage, which occurred in late Pontus time, reactivated a N90º-striking Riedel fault to form the present-day NAF. The South Tosya block began to move westward inducing compression and WSW-directed movement of the North Tosya block (Fig. 8b). This stage has led to the separation of the Kargi and Tosya basins. The third stage, dated as Holocene, is defined by regional southwestward displacements along the DCFZ, which have resulted in the formation of two dextral pull-apart type basins along the Devrez Cay valley bordering the south of the Tosya basin (Fig. 8c).

All our observations made in the field along major faults are compatible with the above model. Striation measurements in sites 12, 13, 14, 15, 16, and 17 (Figs. 5 and 6), located within the Tosya basin, were taken on minor faults affecting Pontus rocks and are more representative of local strain than of main block movements. Inversion of these data give PHI-values close to 0, i.e. norm value of σ_2 close to that of σ_3, which can be interpreted in terms of subsidence of the basin (Fig. 6). This pattern is especially well expressed is the Kargi basin where Holocene sediments cover the major part of the area.

7. Finite displacement estimates and conclusions

The distance between the northern and southern borders of the b1 basin (A_1B_1 in Fig. 8c) approximates the maximum finite motion along the N240º trend paralleling the DCFZ. The estimate for the Holocene time is 13 km which, projected on the N90º-NAF line, yields a 11.2 km dextral offset component. But pull-apart basins generally increase in length by internal deformation. This is the case for the b1 basin because b2 is shorter albeit formed nearby at the same time along the same fault as b1. The length of b2 (A_2B_2 in Fig. 8c) is 6.8 km, corresponding to a 5.9-km component along the NAF. The maximum of displacement of the South Tosya block relative to the Pontides for the Holocene time is consequently 5.9 km, consistent with the 8 km of finite displacement for the same time interval measured by Barka and Hancock (1984) in the area.

The offset between the Tosya and Kargi basins along the N90º-NAF is 12.2 km (CE = DF in Fig. 8c). The two basins having been opened in the early Pontus, this displacement occurred mainly during late Pontus–Quaternary time. For this same time interval, Barka and Hancock (1984) have estimated a 25-km right-lateral displacement.

The maximum amount of opening of the Tosya–Kargi basin in early Pontus time (Tortonian) along

Fig. 8. Geodynamic model of the Tosya area. (a) Lower Pontus (Tortonian). (b) Upper Pontus (Pliocene–Middle Pleistocene). (c) Holocene. *A–B* = Holocene offset responsible for opening of the b1 and b2 pull-apart type basins along the Devrez Cay fault zone; *C–E* and *D–F* = equal upper Pontus–Quaternary offsets respectively of the Tosya fault and Devrez Cay fault zone; GH = Lower Pontus displacement of the North Tosya block along the N70º-NAF/Kargi fault.

the N70º-NAF is the length of segment HG, yielding 14.5 km.

The minimum motion along the NAF can be estimated by the offset of the main valleys (Figs. 5 and 7), yielding 7.5 to 8.5 km. Comparing these values with the above results indicates that they are close to the amount of displacement for the Holocene alone and suggests that the concerned valleys were formed during the Holocene.

The N90º-NAF was not formed before the late Pontus (5.5 Ma for Barka and Hancock, 1984). Prior to that time, there was a proto-NAF segment including the N70º-NAF and the Kargi fault. The DCFZ, which is not parallel to the NAF, has taken the main part of the motion during the Holocene. Our kinematics model is that of independent blocks moving toward the southwest, the west-southwest or the west. Such tectonic movements relatively oblique to the NAF imply that this fault does not strictly obey a model of an intracontinental transform fault along which upper crustal block motions must be parallel to its trace.

Acknowledgements

This work has been carried out in a joint project between Hacettepe University of Ankara and University of Paris VI. The French Embassy and Hacettepe University in Ankara, CNRS and the ‘Ministère des Affaires Etrangères’ in Paris sponsored the field work. ERS1 radar data have been provided by the ESA (project AO2-F112; Jean Chorowicz, Principal Investigator) and processing expenses were partly supported by the CNES. We are grateful to J.F. Dewey and an anonymous reviewer for valuable comments and suggestions that largely improved the quality of the manuscript.

References

Andrieux, J., Over, S., Poisson, A., Bellier, O., 1995. The North Anatolian Fault Zone: distributed Neogene deformation in its northward convex part. Tectonophysics 243, 135–154.

Angelier, J., 1984. Tectonic analysis of fault slip data sets. J. Geophys. Res. 89, 5835–5848.

Angelier, J., 1990. Inversion of field data in fault tectonics to obtain the original stress. A new rapid direct inversion method by analytical means. Geophys. J. Int. 1003, 363–376.

Barka, A.A., 1985. Geology and tectonic evolution of some Neogene–Quaternary basins in the North Anatolian Fault zone. In: The Ketin Symposium. Spec. Publ. Geol. Soc. Turkey, pp. 209–227.

Barka, A.A., 1992. The North Anatolian Fault Zone. Ann. Tectonicae 6, 164–195.

Barka, A.A., 1996. Slip distribution along the North Anatolian fault associated with the large earthquakes of the period 1939–1967. Bull. Seismol. Soc. Am. 86, 1238–1254.

Barka, A.A., Hancock, P.L., 1984. Neotectonic deformation patterns in the convex-northwards arc of the North Anatolian Fault zone. In: Dixon, J.F., Robertson, A.M.F. (Editors), The Geological Evolution of the Eastern Mediterranean. Geol. Soc. London Spec. Publ., 17, pp. 763–774.

Bellier, O., Över, S., Poisson, A., Andrieux, J., 1997. Recent temporal change in the stress state and modern stress field along the North Anatolian Fault Zone (Turkey). Geophys. J. Int. 131, 61–86.

Chorowicz, J., Luxey, P., Lyberis, N., Carvalho, J., Parrot, J.-F., Yürür, T., Gündogdu, N., 1994. The Maras Triple Junction (Southern Turkey) based on Digital Elevation model and satellite imagery interpretation. J. Geophys. Res. 99, 20225–20242.

Chorowicz, J., Luxey, P., Yürür, T., Rudant, J.-P., Gündogdu, N., Lyberis, N., 1995. Slip motion estimation along the Ovacik fault near Erzincan (Turkey) using ERS1 radar image. Remote Sensing Environ. 52, 66–70.

Dewey, J.F., Hempton, M.R., Kidd, W.S.F., Saroglu, F., Sengör, A.M.C., 1986. Shortening of continental lithosphere: the tectonics of Eastern Anatolia — young collision zone. In: Coward, J., Ries, A.C. (Eds.), Collision Tectonics. Spec. Publ. Geol. Soc. London, 19, pp. 3–36.

Dhont, D., Chorowicz, J., Yürür, T., Froger, J.-L., Köse, O., Gündogdu, N., 1998. Emplacement of volcanic vents and geodynamics of Central Anatolia, Turkey. J. Volcanol. Geotherm. Res. (in press).

Hancock, P.L., Barka, A.A., 1980. Plio–Pleistocene reversal of displacement on the North Anatolian fault zone. J. Struct. Geol. 3, 383–392.

Hancock, P.L., Barka, A.A., 1981. Opposed shear senses inferred from neotectonic mesofracture systems in the North Anatolian Fault Zone. J. Struct. Geol. 5, 217–220.

Irrlitz, W., 1971. Neogene and older Pleistocene of the intermontane basins in the Pontic region of Anatolia. Newsl. Stratigr. 1 (3), 33–36.

Irrlitz, W., 1972. Lithostratigraphie und Tektonische Entwicklung des Neogens in Nordostanatolien. Beih. Geol. Jahrb. 120, 1–111.

Le Pichon, X., Chamot-Rooke, N., Lallement, S., Noomen, R., Veis, G., 1995. Geodetic determination of the kinematics of central Greece with respect to Europe: implications for eastern Mediterranean tectonics. J. Geophys. Res. 100, 12675–12690.

McKenzie, D.P., 1972. Active tectonics of the Mediterranean region. J.R. Astron. Soc. 30, 109–185.

Oral, B., Reilinger, R.E., Toksoz, M.N., King, R.W., Barka, A.A., Kinik, I., Lenk, O., 1995. Global Positioning System offers evidence of plate motions in eastern Mediterranean. Eos 76, 2.

Över, S., 1996. Analyse tectonique des états de contrainte cénozoïques dans la zone centrale de la Faille Nord Anatolienne. Ph.D. Thesis, University of Paris-Sud, Orsay.

Över, S., Poisson, A., Temiz, H., Andrieux, J., 1992. La tectonique récente dans le bassin de Tosya (partie centrale de la Faille Nord Anatolienne, Turquie). Bull. Fac. Eng. Cum. Univ., Série A 9 (1), 3–10.

Över, S., Bellier, O., Poisson, A., Andrieux, J., Tutkun, Z., 1993. Esquisse de l'évolution néogène à actuelle de l'état de contrainte dans la partie centrale de la Faille Nord Anatolienne (Turquie). C.R. Acad. Sci. Paris, Sér. II 317, 827–833.

Reilinger, R.E., McClusky, S.C., Oral, M.B., King, R.W., Toksoz, M.N., Barka, A.A., Kinik, I., Lenk, O., Sanli, I., 1997. Global Positioning System measurements of present-day crustal movements in the Arabia–Africa–Eurasia plate collision zone. J. Geophys. Res. 102, 9983–9999.

Sengör, A.M.C., 1979. The North Anatolian transform fault: its age, offset and tectonic significance. J. Geol. Soc. Am. 136, 269–282.

Sengör, A.M.C., Görur, N., Saroglu, F., 1985. Strike-slip faulting and related basin formation in zones of tectonic escape: Turkey as a case of study. In: Biddle, K.T., Christie-Blick, N. (Eds.), Strike-slip Faulting and Basin Formation. Soc. Econ. Paleontol. Mineral. Spec. Publ. 37, 227–264.

Stein, R.S., Barka, A.A., Dieterich, J.H., 1997. Progressive failure on the North Anatolian fault since 1939 by earthquake stress triggering. Geophys. J. Int. 128, 594–604.

Suzanne, P., Lyberis, N., Chorowicz, J., Nurlu, M., Yürür, T., Kasapoglu, E., 1990. La géométrie de la Faille Nord Anatolienne à partir d'images Landsat-MSS. Bull. Soc. Géol. Fr. 8, 589–599.